

Computer-aided comprehensive explorations of RNA structural polymorphism through complementary simulation methods

Konstantin Röder¹, Guillaume Stinermann², Pietro Faccioli³, and Samuela Pasquali^{4,5*}

¹Yusuf Hamied Department of Chemistry, University of Cambridge, Cambridge, UK

²CNRS Laboratoire de Biochimie Théorique, Institut de Biologie Physico-Chimique, PSL University, Université de Paris, 13 rue Pierre et Marie Curie, 75005, Paris, France

³Department of Physics, University of Trento and INFN-TIFPA, Trento, Italy

⁴Laboratoire CiTCoM, CNRS UMR 8038, Université Paris Cité, 4 avenue de l'Observatoire, 75006, Paris, France

⁵Laboratoire BFA, CNRS UMR 8251, Université Paris Cité, 35 rue Hélène Brion, 75013, Paris, France

*Corresponding author. Email: samuella.pasquali@u-paris.fr

Abstract

While RNA folding was originally seen as a simple problem to solve, it has been shown that the promiscuous interactions of the nucleobases result in structural polymorphism, with several competing structures generally observed for non-coding RNA. This inherent complexity limits our understanding of these molecules from experiments alone, and computational methods are commonly used to study RNA. Here, we discuss three advanced sampling schemes, namely Hamiltonian-replica exchange molecular dynamics, ratchet-and-pawl molecular dynamics and discrete pathsampling, as well as the HiRE-RNA coarse-graining scheme, and highlight how these approaches are complementary with reference to recent case studies. While all computational methods have their shortcomings, the plurality of simulation methods

This peer-reviewed article has been accepted for publication but not yet copyedited or typeset, and so may be subject to change during the production process. The article is considered published and may be cited using its DOI.

10.1017/qrd.2022.19

This is an Open Access article, distributed under the terms of the Creative Commons Attribution-NonCommercial-NoDerivatives licence (<http://creativecommons.org/licenses/by-nc-nd/4.0/>), which permits non-commercial re-use, distribution, and reproduction in any medium, provided the original work is unaltered and is properly cited. The written permission of Cambridge University Press must be obtained for commercial re-use or in order to create a derivative work.

28 leads to a better understanding of experimental findings and can inform and guide
29 experimental work on RNA polymorphism.

30

31 **The complexity of RNA folding**

32 After the seminal experiments showing the hierarchical folding of RNA, RNA folding was
33 thought to be an easier problem to solve than protein folding (Li, Viereg, et al. 2008;
34 Tinoco and Bustamante 1999). With an alphabet composed of only four letters, and with
35 key interactions leading to the observed secondary structure dictated by canonical base
36 pairing (G with C and A with T/U), what remained to be solved was “only” a combinatorial
37 problem of finding the best pairing scheme for a given sequence.

38 About two decades later, we know that the problem is much more complex. Even
39 searching for the optimal secondary structure remains a challenge as exhaustive sampling
40 of all relevant conformations is unfeasible for most systems of biological interest, even
41 though the advent of machine learning and the extensive use of chemical probing data are
42 contributing to making the problem more tractable (Lorenz et al. 2016; Zhao et al. 2021).
43 A common feature in complex RNA architectures are pseudoknots – non-nested
44 arrangements of base pairs. Traditional secondary structure prediction algorithms do not
45 treat these structures well and combining these approaches with machine learning has led
46 to some progress (Sato and Kato 2022; Wang, Liu, et al. 2019). The situation is even more
47 complex considering that canonical base pairing, even though dominant, is not the only
48 form of base pairing. The multiple hydrogen bond donor and acceptor sites of the
49 nucleobases allow for a multitude of base pairs, which have been reported experimentally.
50 Around 150 non-canonical base pairs have been found and classified in terms of
51 interaction “edges” (Watson-Crick, Hoogsteen and Sugar) (Leontis and Westhof 2001;
52 Stombaugh et al. 2009). The full list can be found in the RNA Basepair Catalog of the
53 Nucleic Acids Databank.

54 As it is the case in general for heteropolymers, a smaller alphabet results in an increase
55 of frustration of the conformational space accessible to the molecule. In the case of RNA,
56 the alphabet composed of only four different nucleobases, further complicated by the
57 multitude of possible base pairs, results in a folding process possibly more complex to
58 predict than for proteins (Ferreiro et al. 2014). The observation that proteins fold reliably
59 and fast into their native confirmation has been explained by the principle of minimal
60 frustration (Bryngelson and Wolynes 1987). Every sequence defines interactions between
61 different parts of the molecule. The more of these are formed, the lower the frustration
62 and the more stable the resulting structure. The native state exhibits a conformation that
63 fulfils all packing requirements, i.e. the system shows minimal frustration. Minimal
64 frustration is linked to the topography of the energy landscape, and in the case of globular
65 proteins a single funnel anchored around the native fold is observed (Bryngelson, Onuchic,

66 et al. 1995; Leopold et al. 1992).¹ As a result, the number of native contacts observed is a
67 good proxy for the progress of the highly cooperative folding of proteins.

68 In contrast, RNA is characterized by the existence of several stable structural
69 ensembles with different secondary structures, and many of these systems are highly
70 dynamic (Brillet et al. 2020). The number of alternative contacts in RNA lead to large
71 frustration and disorder, as the sequence allows for multiple competing interactions. This
72 higher frustration has been highlighted both by experiments (Burge et al. 2006; Garst et
73 al. 2011; Kolesnikova and Curtis 2019; Lightfoot et al. 2019; Martinez-Zapien et al. 2017;
74 Saldi et al. 2021; Yu et al. 2021) and by simulations (Cragnolini, Laurin, et al. 2015;
75 Denesyuk and Thirumalai 2011; Rissone et al. 2022; Röder, Barker, et al. 2022; Röder,
76 Stirnemann, et al. 2020; Schlick et al. 2021; Šponer et al. 2018; Yan et al. 2022), and its
77 main manifestation is structural polymorphism. Within these distinct structures, there
78 must not necessarily be a distinct global minimum, and therefore a native state does not
79 necessarily exist, as has been noticed by others (Vicens and Kieft 2022).

80 Therefore, in our opinion, an ensemble approach should be chosen when talking about
81 RNA. The relative population of these structural ensembles depends on experimental
82 conditions, as observed for riboswitches and several other non-coding regulatory RNAs
83 (Brillet et al. 2020; Fay et al. 2017; Halvorsen et al. 2010; Kolesnikova and Curtis 2019).
84 Post-transcriptional modifications and single point mutations also can shift the
85 equilibrium between the alternative structures (Liu et al. 2017; Martinez-Zapien et al.
86 2017; Röder, Barker, et al. 2022; Schlick et al. 2021). Finally, many RNAs interact with
87 proteins and these interactions often lead to changes to the observed fold (Jaeger et al.
88 2009). Which structure is detected in experiments therefore depends on the details of the
89 experiment itself, and at times more than one structure is detected in the same experiment
90 (Martinez-Zapien et al. 2017).

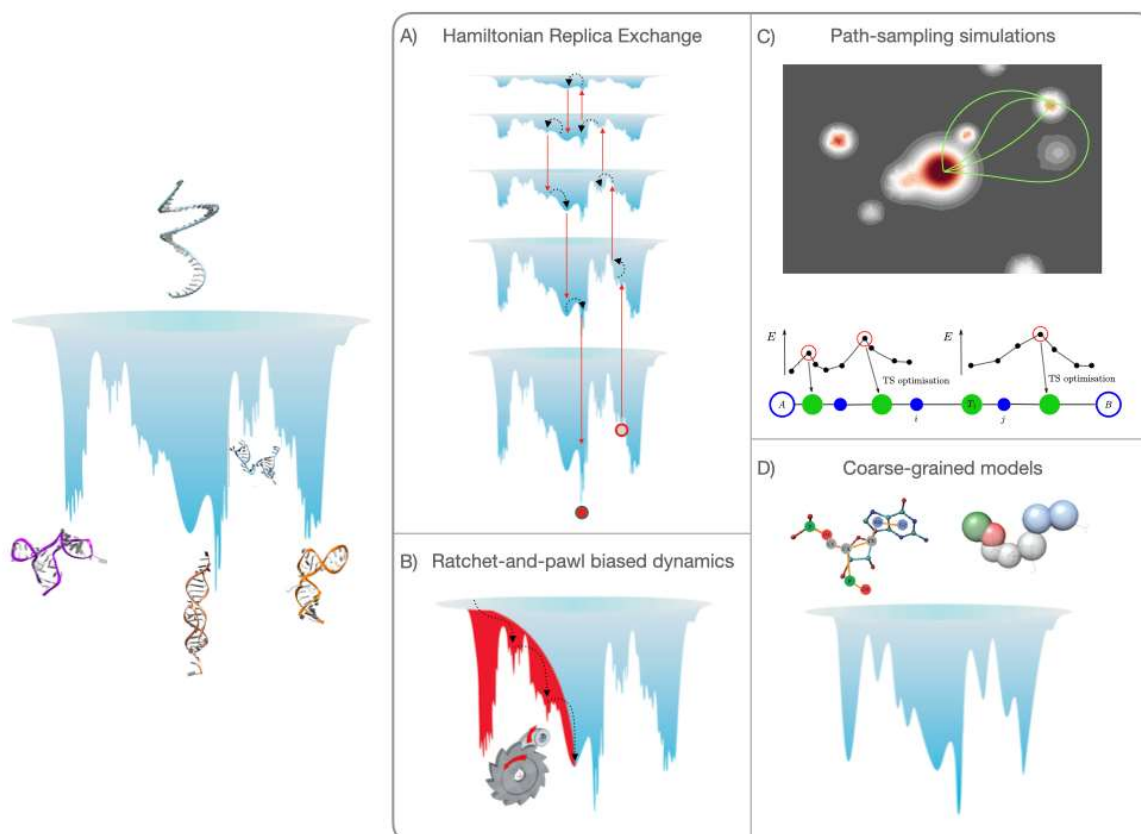
91 Given this plurality of possible structures, simulations cannot be limited to the
92 prediction of a single structure (which is what is achieved by most bioinformatic
93 approaches), and focus must shift to a global view, which centres around the molecular
94 energy landscape. All information about the structures, their energy, and interconversion
95 pathways between them can be calculated from knowledge of the energy landscape (EL).
96 Insight can also be obtained on the influence of external factors such as ionic conditions,
97 pH, temperature, presence of ligands, and chemical changes in the sequence by
98 considering the EL. Any experiment or simulation probes the energy landscape directly or
99 indirectly. Various methods do so in different ways, and often the EL is not directly
100 mapped.

101 The most common simulation method is molecular dynamics (MD) simulations.
102 However, due to the broken ergodicity exhibited biomolecular energy landscapes (Wales
103 and Salamon 2014) there are many practical difficulties. In brief, the structural ensembles
104 are separated by high barriers, making transitions between them rare events. This kinetic

¹ This description extends to proteins that exhibit more than one structural ensemble, and which have a multifunnel energy landscape. Such landscapes are also governed by the principle of minimal frustration (Röder and Wales 2018).

105 partition between different regions will make observation of transitions in standard MD
 106 simulations very unlikely. As a result, so called enhanced sampling approaches have been
 107 developed, which for example include pathsampling methods.

108 Here, we present our perspective on how simulations can be used to gather information
 109 on RNA energy landscapes and structural polymorphism. There are two approaches
 110 commonly employed. The first option is the use of enhanced sampling methods (Mlýnský
 111 and Bussi 2018), and here we briefly present three of these, namely Hamiltonian Replica
 112 Exchange (H-REX, REST2) simulations (Wang, Friesner, et al. 2011), discrete
 113 pathsampling (DPS) (Wales 2002; Wales 2004) and a variationally optimized ratchet-and-
 114 pawl molecular dynamics (rMD) simulation scheme (Tiana and Camilloni 2012) called
 115 Bias Functional approach (A Beccara et al. 2015). The second option is to smooth the
 116 energy landscape through coarse-graining (Papoian 2018). A pictorial illustration on how
 117 each of these methods samples the energy landscape is given in Fig.1. By considering
 118 several examples, we show that these approaches are complementary, and that the best
 119 results are obtained when combining multiple simulation methods.



120

121 *Figure 1: Left: Illustration of how the energy landscape of a polymorphic RNA might look like (the*
 122 *vertical axis represents the energy or free energy of the system). At the top of the landscape,*
 123 *we find high energy unfolded conformations, while we note several deep minima, separated*
 124 *by high barriers, all corresponding to substantially different structures of the molecule. One*

125 *of these minima might be observed experimentally and referred to as the “native structure”.*
126 *Right panel (A-D): illustration of how each of the method presented samples the landscape.*

127

128 **An overview of the simulation methods**

129 **Hamiltonian-Replica Exchange simulations**

130 Despite the increased time scales that can be probed with unperturbed MD simulations –
131 now routinely on the order of μs – the relevant conformational motions cannot be sampled
132 as the associated time scales still exceed computational feasibility, prompting interest for
133 enhanced sampling strategies that have been developed and widely applied to
134 biomolecules, including RNA (see e.g. Mlýnský and Bussi 2018 for a recent review).

135 One way to improve sampling in an unguided way (i.e. without assuming or imposing
136 predetermined collective variables along which the transitions will occur) is through the
137 use of replica exchange MD simulations (Sugita and Okamoto 1999). Multiple copies of the
138 system are simulated at different temperatures, increasing the accessible time scales.
139 However, this approach is very sensitive to the overlap between the replicas, which
140 depends on the number of degrees of freedom, and at the moment it is hardly applicable
141 at an all-atom resolution for nucleic acids exceeding a handful of residues in explicit
142 solvent.

143 This problem may be overcome by using Hamiltonian replica-exchange (H-REX)
144 simulation schemes. In particular, we used the Replica-Exchange with Solute Tempering
145 (REST2) strategy (Wang, Friesner, et al. 2011), where all replicas evolve at the same
146 physical temperature, but they can exchange their Hamiltonian with a scaled potential
147 energy for the biomolecule (Fig.1A), decreasing the number of degrees of freedom. As a
148 result, fewer replicas are required, and sampling is enhanced. For example, for proteins
149 containing 100-200 residues, one to two dozen replicas were shown to lead to satisfactory
150 exchange probabilities (Maffucci, Laage, Sterpone, et al. 2020; Maffucci, Laage,
151 Stirnemann, et al. 2020; Stirnemann and Sterpone 2017). However, this technique has
152 mostly been applied to short oligonucleotides, and in particular to the sampling of
153 tetraloops conformational space (Bottaro et al. 2020; Kührová et al. 2016; Mlýnský,
154 Janeček, et al. 2022). While a recent work pointed to limitations in the ability of such an
155 approach to actually fold even short RNAs (Mlýnský, Janeček, et al. 2022), REST2 remains
156 a very attractive strategy to ease and to accelerate conformational sampling, which
157 eventually enables to escape the kinetic traps in which brute-force simulations may be
158 stuck for long times.

159 In this short perspective, we exclusively focus on REST2, which we have applied to an
160 RNA much larger than these tetraloops (Röder, Stirnemann, et al. 2020), but other
161 applications to reasonably large biomolecules are mostly limited to DNAs and proteins.
162 For these applications, recent success of REST2 in identifying important conformations
163 that were not revealed by long brute-force MD (Gillet et al. 2021; Maffucci, Laage,
164 Sterpone, et al. 2020; Maffucci, Laage, Stirnemann, et al. 2020; Stirnemann and Sterpone

165 2017) offer promising perspectives for the RNA field. However, it should be noted that
166 when employed with atomistic resolution models, the computational costs remain high.
167 This shortcoming may be overcome by focusing on a specific region of the system under
168 investigation, reducing the size of the perturbed region, and thus the number of required
169 replicas.

170 **Ratchet-and-pawl molecular dynamics (rMD) and the Bias Functional** 171 **approach**

172 Ratchet-and-pawl (rMD) simulations are based on introducing a soft history-dependent
173 biasing force to enhance the generation of productive folding trajectories towards a given
174 target structure (Paci and Karplus 1999). In practice, once a target structure is known
175 experimentally, it is possible to extract some features characteristics of its configuration
176 and define a collective variable that can be used to guide unfolded structures toward it in
177 a biased molecular dynamic simulation. In the literature, many collective variables exist
178 for biomolecules, ranging from a simple atomic distance or dihedral angle to the radius of
179 gyration, the RMSD and many more depending on the specific feature relevant for the fold
180 of the molecule (Fiorini et al. 2013). The system is free to explore the energy landscape, as
181 long as it follows broadly this predetermined collective variable (CV), which is a proxy for
182 the reaction coordinate. An external biasing force is switched on when the system
183 backtracks with respect to the CV (see Fig.1B). In RNA and protein folding simulations,
184 one choice for the predetermined CV is obtained from the overlap of the instantaneous
185 and the target atomistic contact map (Camilloni et al. 2011). This approach produces
186 folding trajectories efficiently but requires structural information about the target.

187 In the ideal case in which CV coincides with the reaction coordinate (the committor
188 function (E and Vanden-Eijnden 2010)), rMD trajectories sample the correct region of
189 configuration space (Bartolucci et al. 2018; Cameron and Vanden-Eijnden 2014).
190 However, the choice of CV used in RNA folding simulations is only a proxy of the ideal
191 reaction coordinate. Therefore, with rMD it is only possible to obtain an approximate
192 reconstruction of the folding energy landscape. Systematic errors from the biasing force
193 can be minimised by applying Bias Functional (BF) filtering procedure (A Beccara et al.
194 2015). In this approach, a variational principle derived from the path integral
195 representation of Langevin dynamics (Onsager and Machlup 1951) is used to select the
196 folding trajectories generated by rMD that have the highest probability of occurring in the
197 absence of any biasing force.

198 Apart from the requirement to use structural information about the folded structure,
199 another drawback of rMD simulations is that the generated trajectories only explore part
200 of the energy landscape, namely the region most likely traversed by productive pathways
201 towards the predetermined target structure. While this approach greatly enhances
202 computational efficiency, it prevents the method from exploring other parts of the
203 landscape that may be associated with kinetic trapping.

204 **Discrete pathsampling for RNA**

205 H-REX and rMD simulations compute trajectories of molecules moving on the energy
206 landscape. Discrete pathsampling (DPS) (Wales 2002; Wales 2004) focuses on the
207 topography of the energy landscape. The energy landscape is considered coarse-grained,
208 where only the local minima and transition states that connect them are used as
209 representation. Each transition state connects two local minima, and between any pair of
210 minima, we can identify a discrete path consisting of a series of minima connected by
211 transition states. This representation results in a kinetic transition network, which can
212 then be analysed to obtain kinetic and thermodynamic characteristic, including the
213 associated structures and transition mechanisms.

214 Through this approach, the topography of the energy landscape is obtained, and this
215 information allows readily for interpretation of mutational data (Röder, Stirnemann, et al.
216 2020). As local minima and transition states are well-defined geometrically, they can be
217 located by geometry optimisation, overcoming the dependence on long time scales other
218 simulations suffer from. A shortcoming of the method is the use of implicit solvent
219 representations, which introduces a source of error (Šponer et al. 2018). While it is
220 theoretically possible to use explicit solvent, the increased computational cost currently
221 prevents such setups. While free energies can be readily obtained, explorations of higher
222 entropy configurations are difficult. As such, structural transitions between folded
223 structures are generally well resolved, while unfolding events are not. More information
224 and details on how the energy landscapes are explored with DPS can be found in various
225 reviews (Joseph et al. 2017; Röder, Joseph, et al. 2019).

226 While DPS is most efficient when folded structures are known, the methodology can
227 locate unknown folded structures and new funnels, as demonstrated in the exploration of
228 mutational changes for example in 7SK RNA (Röder, Stirnemann, et al. 2020). However,
229 currently there is no algorithm to guarantee the location of all structures. A useful way
230 around this limitation is to create several possible alternative structures and connect
231 them. Importantly, this approach does not require the structures to be optimised as long
232 as key interactions, such as base pairs are formed.

233 **Coarse-grained RNA representations**

234 By grouping several atoms into larger particles (grains), the computational exploration of
235 the energy landscape is aided in two ways. Firstly, the coarse-graining smooths the energy
236 landscape (see Fig.1D), which removes kinetic traps for the exploration. Secondly, the
237 number of degrees of freedom is reduced, making the computations more tractable. The
238 choice of the mapping between atoms and grains depends on the level of details required
239 and on the kind of interactions that are considered relevant (see (Li and Chen 2021) for a
240 recent review on the different existing RNA coarse-grained models). For RNA structures,
241 key elements are base pairing, stacking and electrostatic interactions. In the HiRE-RNA
242 model (High-Resolution Energy model for RNA) (Cragolini, Laurin, et al. 2015; Pasquali
243 and Derreumaux 2010), we have chosen to preserve a relatively high resolution with each

244 nucleotide described by 6 or 7 beads. This level of detail, while significantly reducing the
 245 number of particles, allows the definition of planes for the nucleobases, reflecting the
 246 aromatic rings stacking, and distinguishes different edges of the bases to account for both
 247 canonical and non-canonical pairings. While using an implicit solvent, long-range
 248 electrostatic effects are accounted for by a Debye-Hückel potential energy term dependent
 249 on experimental ionic concentrations in solution. While the development of this coarse-
 250 grained model is still on-going, its usefulness for small systems (Cragolini, Chakraborty,
 251 et al. 2017; Stadlbauer et al. 2016) and when coupled to experimental data (Mazzanti et
 252 al. 2021; Pasquali, Frezza, et al. 2019) has been demonstrated.

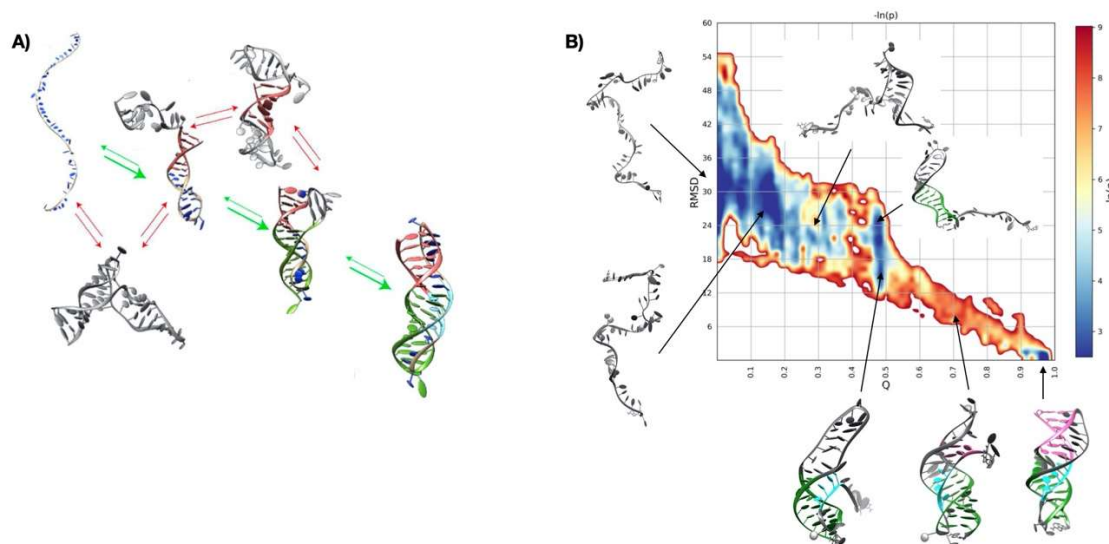
253 The obvious shortcoming of any coarse-graining (CG) methodology is the loss of detail,
 254 due to the lower model resolution. In addition, the implicit nature of solvent and ions will
 255 impact the observed features. These drawbacks mean the entropy is not faithfully
 256 produced within coarse grained simulations. However, the reduced complexity will allow
 257 the study of larger systems and larger scale rearrangements, providing otherwise
 258 inaccessible insights.

259 Despite the fewer degrees of freedom, our coarse-grained MD simulations can still be
 260 expensive, with several days of CPU needed to achieve folding of a small molecule of 20-
 261 30 nucleotides, although we will be able to achieve much greater speed once the force-
 262 field will be ported to parallel MD computing.

263 A small showcase

264 In this section, we discuss a few illustrative applications of these methods, emphasising
 265 their complementary nature.

266



267

268 *Figure 2: Folding of the human telomerase triple helix performed with unbiased coarse-grained*
 269 *simulations (REMD), allowing to widely explore alternative conformations (A) and with*
 270 *biased atomistic simulations allowing to explore the details of intermediate states (B).*

271 Folding pathway of the human telomerase H-pseudoknot triple helix

272 This example is a 47-nucleotide RNA, exhibiting a H-pseudoknot (two-interlacing strands)
273 further stabilized by a triple helix (PDB ID 2K96). The system has been studied extensively
274 experimentally (Gavory et al. 2006; Kim et al. 2008; Theimer et al. 2005) and has become
275 a benchmark for modelling (Biyun et al. 2011; Cho et al. 2009; Denesyuk and Thirumalai
276 2011), as it contains a pseudoknot, a challenging structural feature, and non-canonical
277 interactions leading to triplet formation in the triple helix. This system was also used as
278 test case for the HiRE-RNA model (Cragolini, Laurin, et al. 2015), and, more recently, to
279 validate the application of variationally optimized rMD to RNAs (Lazzeri et al. 2022).
280 Folding simulations were performed in both instances starting from fully unfolded
281 conformations.

282 The coarse-grained simulations consisted of a long run with the HiRE-RNA model and
283 replica exchange MD simulations at 64 different temperatures. rMD folding simulations
284 consisted of 100 short runs (each lasting a nominal time interval of 5 ns) with the AMBER
285 ff99 with the Barcelona α/γ backbone modification (Perez et al. 2007) and the χ
286 modification (Zgarbova et al. 2011). It should be emphasized that the simulation time does
287 not directly correlate with the physical transition path time, as the history-dependent bias
288 brakes microscopic reversibility and alters the kinetics. CG simulations required two
289 weeks of computation on local cluster in 2015 to achieve the native structure for the first
290 time. rMD simulations required roughly a week of simulation to generate all trajectories
291 on a GPU cluster in 2022. The results of the two simulations are shown in Fig.2.

292 The HiRE-RNA simulations yielded the correct native state and identified a sensible
293 folding pathway. Moreover, alternative states were observed, which constitute kinetic
294 traps and are characterized by the formation of non-native secondary structures, leading
295 to alternative folds. These results were in qualitative agreement with experimental
296 evidence of the formation of metastable states and folding intermediates (Kim et al. 2008).
297 Despite the coarse-graining, these simulations were computationally expensive and the
298 sampling was not optimal. In particular, it was not possible to give a full assessment of the
299 relative populations of the observed states. The rMD simulations produced more insight
300 into the productive folding pathway to the experimentally observed target structure. It
301 was possible to collect statistically relevant populations for the different conformations
302 and generate a heatmap illustrating the folding in terms of formation of native contacts
303 and RMSD with respect to target (see Fig.2B). The results highlighted the ruggedness of
304 the folding landscape, characterized by a multitude of intermediate states. Moreover, we
305 were able to infer the existence a pronounced bottleneck towards the final stage of folding,
306 when the formation of the pseudoknot takes place. It was also possible to characterize the
307 order of the events of folding in terms of formation of stems and loops and the main path
308 found by our simulations corresponded well with the experimental evidence from
309 thermodynamic studies (Kim et al. 2008) and by simulations by other groups (Cho et al.
310 2009).

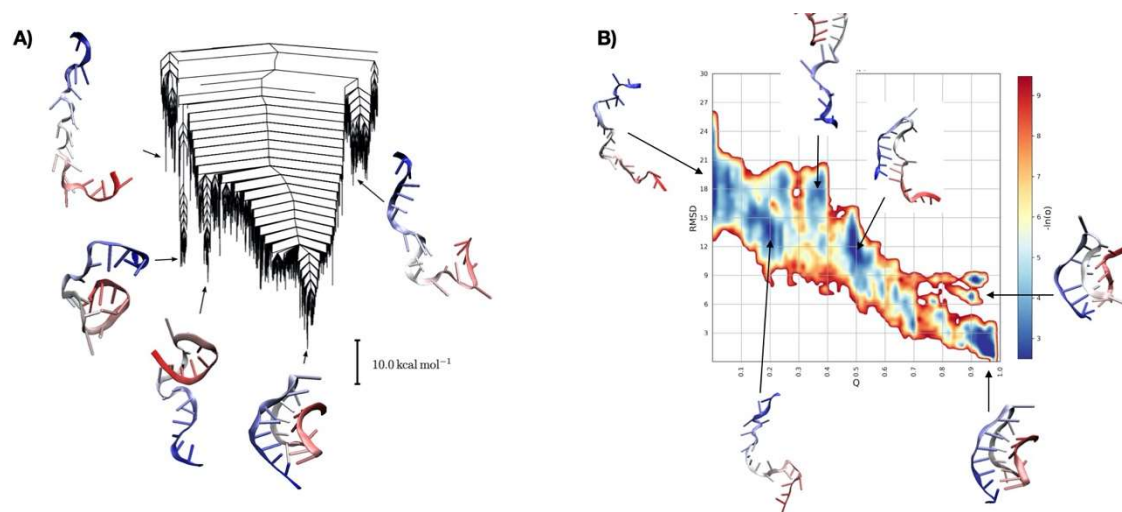
311 Importantly, both methods lead to the correct folding path and folding intermediates,
 312 giving credibility to both methods. In addition, the unbiased CG simulations also identified
 313 alternative structures, which are not on the folding pathway. The rMD simulations can
 314 provide statistics of the explored states and detailed insight into the interactions along the
 315 folding pathway.

316 Energy landscape and folding pathway of a small H-pseudoknot

317 For the 22-nucleotide long tmRNA pseudoknot taken from *Aquifex aeolicus* (PDB ID
 318 2G1W) (Nonin-Lecomte et al. 2006), we performed both a full exploration of the energy
 319 landscape with discrete pathsampling and an exploration of the folding pathway with rMD
 320 (see Fig.3). Both sets of simulations used the atomistic AMBER ff99 force field with the
 321 Barcelona α/γ backbone modification and the χ modification (Zgarbova et al. 2011). The
 322 energy landscape exploration used an implicit solvent model, while the rMD simulations
 323 were in explicit solvent.

324 As the system is small (in fact, it is the smallest known pseudoknot), it was possible to
 325 exhaustively explore the energy landscape (Ma et al. 2021). From these simulations, we
 326 can again appreciate the presence of a rugged folding funnel (see Fig.3A). The energy
 327 landscape is characterized by one main funnel anchored by the native, experimentally
 328 observed structure. Some smaller subfunnels exist on the energy landscape, but only small
 329 barriers separate them from the main funnel. When analysing the ensemble of structures
 330 corresponding to these subfunnels, we detect partially folded states, but no states with
 331 alternative secondary structure competing with the native fold. The rMD simulations
 332 provided insight into the folding mechanism. As in the previous case, the folding pathways
 333 cross a multitude of metastable intermediate states (see Fig.3B).

334
 335



336
 337 *Figure 3: folding of the small H-pseudoknot PK1 studied with path sampling to obtain its energy*
 338 *landscape (A) and with biased folding simulations to study the native folding mechanism (B).*

339 The two approaches support each other in this conclusion. While DPS provides a
340 complete view of the energy landscape, the interaction with the solvent and the high
341 entropy regions are not fully resolved, and rMD provided the missing details for the
342 folding pathway.

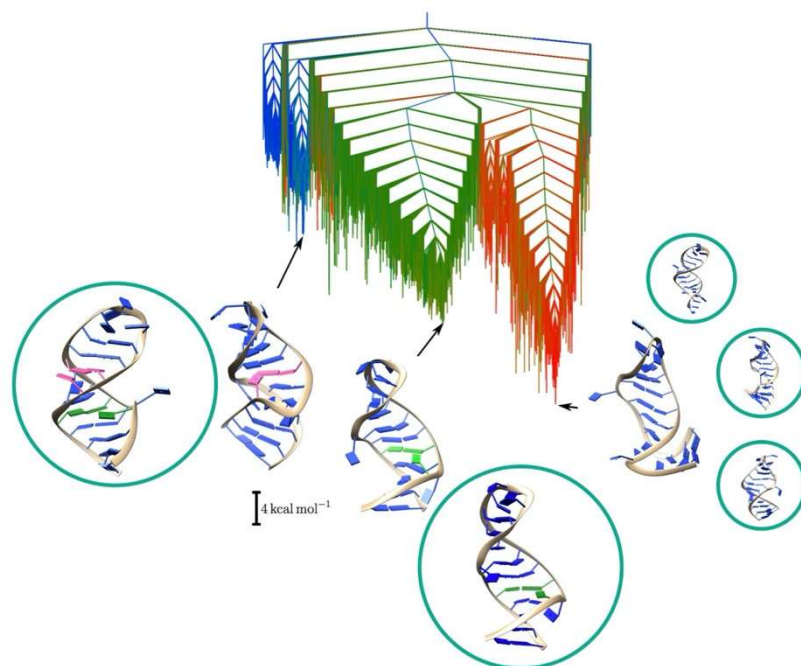
343 **Exploring polymorphism: 7SK RNA and KSHV's ORF50 transcript**

344 7SK RNA is a non-coding RNA and part of a ribonucleoprotein complex, which is crucial to
345 transcription regulation by RNA polymerase II (Wassarman and Steitz 1991). Its 5' hairpin
346 (HP1) was characterized experimentally by different methods including X-ray
347 crystallography (Martinez-Zapien et al. 2017), NMR (Bourbigot et al. 2016), SAXS (Brillet
348 et al. 2020), and chemical probing (Lebars et al. 2010; Olson et al. 2022). As a perfect
349 example of RNA polymorphism, the high-resolution methods (NMR and X-ray) detected
350 substantially different structures for this hairpin, including two distinct structures within
351 the same crystal.

352 The three alternative structures are characterized by a reorganization of base pairing
353 in the upper portion of the stem. The NMR structure is a hairpin with bulges and only
354 canonical base pairing, while the X-ray structures exhibit non-canonical pairings and some
355 triplets, organized differently in the two structures. The hairpin is the binding site for an
356 affector protein (Egloff et al. 2018), which is crucial to the important biological function of
357 RNA 7SK (Nguyen et al. 2001; Yang et al. 2001). Hence, understanding this structural
358 polymorphism and its implication is of significant importance.

359 We used DPS and H-REX simulations to study the upper portion of HP1 (27
360 nucleotides), and further studied a set of mutations (Röder, Stirnemann, et al. 2020),
361 reported to affect the binding affinity of HP1 (Martinez-Zapien et al. 2017). DPS was
362 initiated from the experimentally observed

363
364



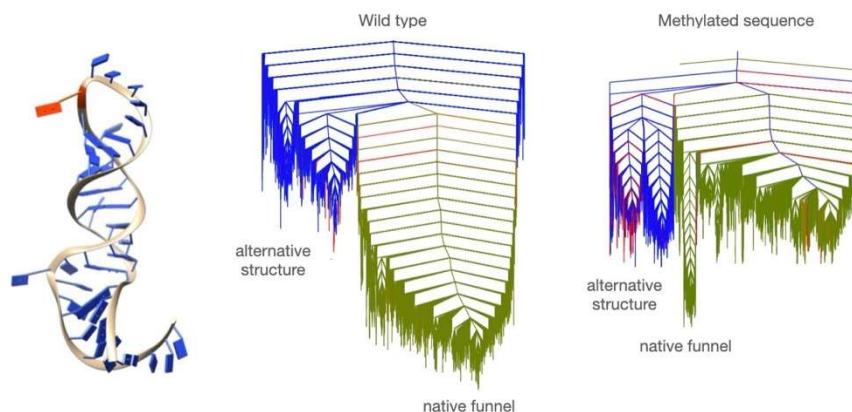
365

366 *Figure 4: Energy landscape obtained from DPS for the 7SK RNA HP1 hairpin with key structures shown.*367 *The structural polymorphism is clearly observable, with three main funnels corresponding*368 *to more compact stem loops as observed in X-ray crystallography (blue and green), and more*369 *extended structures as observed by NMR experiments (red). Encircled structures correspond*370 *to the main clusters observed in H-REX simulations.*

371

372 crystal structures and a multifunnel energy landscape was obtained from sampling,
373 including descriptions of the relative stability and interconversion pathways (see Fig.4).²374 The energy landscape revealed the polymorphic character of the HP1 hairpin, and
375 based on the observed structures and their relative energies, we formulated a hypothesis
376 relating the lowest energy X-ray hairpin structure to the binding of the effector protein.
377 From our exploration of the energy landscapes for various mutants, we were able to draw
378 a correlation between specific mutations and protein binding affinity, providing a
379 mechanical explanation of the observed mutational effects.380 Two sets of H-REX simulations complemented the energy landscape exploration with
381 DPS, each starting from one of the observed crystal structures. Simulations were
382 performed for 100ns using 20 replicas, with a Hamiltonian coupling λ ranging from 1 to 0.
383 Due to the large size of the solvated system (roughly 30,000 atoms), convergence for such
384 simulations is difficult to achieve. Nonetheless, the findings from the extended trajectories
385 agree with the observations from pathsampling. The clusters of structures corresponded
386 well to the structures found in the main funnels of the energy landscape. The agreement
387 between the simulations enabled us to exclude a prominent role of structural water
388 molecules or ions, which is not possible from the implicit solvent representation in used

² A detailed description of how this computational study was conducted is reported in (Röder and Pasquali 2021).



389 in DPS. While DPS did not necessarily explore the high-energy portions of the landscape,
 390 which would require

391 *Figure 5: EL of wild type and methylated sequence for ORF50. One of the lowest energies structures is*
 392 *shown with the site of methylation highlighted in red.*

393

394 unfolding and potential refolding into different structures, the H-REX simulations did
 395 explore these regions. We would therefore expect H-REX to be able to depart more
 396 significantly from the initial structures and possibly find new structures with a full
 397 reorganization of the molecule. In our simulations, however, we only located states
 398 already explored by discrete pathsampling. The experimental evidence combined with the
 399 exploration of two different kind of simulations, give us some confidence that we have
 400 probably explored all the biologically relevant structures of the system.

401 Another area of growing interest is the study of post-translational modifications. In a
 402 recent study we investigated a post-translational methylation of an RNA hairpin (Röder,
 403 Barker, et al. 2022). As many RNAs are subject to methylation (Zaccara et al. 2019), it is
 404 important to understand how this modification impacts the adopted structures and how
 405 the equilibrium between possible alternative structures is altered. In the case of the RNA
 406 transcript of open reading frame 50 (ORF50) of Kaposi's sarcoma-associated herpes virus,
 407 which encodes the replication and transcription activator protein required for viral
 408 activation (Guito and Lukac 2012), methylation stabilises the RNA transcript, leading to
 409 effective viral replication (Baquero-Perez et al. 2019). Here, discrete pathsampling was
 410 used based on experimentally observed secondary structures (Baquero-Perez et al. 2019)
 411 only.

412 Our study revealed the existence of several structural basins, with the native structure
 413 occupying the lowest energy states. A set of higher energy structures, which allow
 414 interactions of the transcript with proteins (in this case a m6A reader), is found as well. In
 415 the unmethylated system, these structures are effectively inaccessible, while the
 416 methylation reduces the energy difference significantly, leading higher occupation of
 417 these states, which can recruit the m6A reader (see Fig.5).

418 These results highlight the importance of studies of mutations and chemical
419 modifications, as the unmodified sequence might exhibit polymorphism, but it cannot be
420 detected in experiment, while small alterations lead to significant changes in the energy
421 landscape, which may lead to detectable polymorphism.

422 **Conclusions and Perspectives**

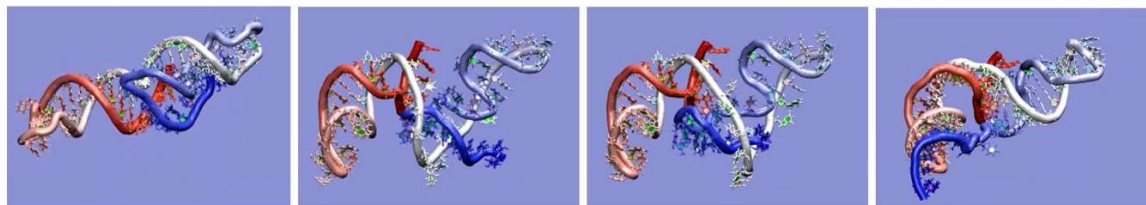
423 From these case studies, we can draw some general conclusions on the specificity of RNA
424 folding and on what can constitute a profitable strategy to tackle larger and more complex
425 systems. For all systems we have studied, even the simplest, we find a rugged energy
426 landscape, i.e it is characterized by the presence of many locally stabilised structures,
427 corresponding to the subsequent formation of local secondary structures. These
428 configurations may be part of a single funnel, most likely for small systems, or, if they
429 exhibit significant difference in their secondary structure, belong to competing funnels, a
430 feature likely observed for larger RNA molecules.

431 A successful strategy to investigate the possible structures is the combination of
432 several simulation methods. Secondary structure predictions based on bioinformatics
433 may already reveal some of the complexity of the RNA folding problem. If a single
434 dominant structure emerges, it is likely that the energy landscape is less complex and
435 exhibits a single main funnel. In such cases, it is likely that canonical base pairs are
436 adopted, and chemical probing may give further confidence in such predictions. Non-
437 canonical interactions may be important to local structural details. Of course, in these
438 scenarios, complexity may arise from additional effects, such as post-translational
439 modifications.

440 If, on the other hand, multiple secondary structures are proposed, a multiscale
441 approach can be useful. Using a coarse-grained model, initial scouting of the energy
442 landscape can yield a survey of possible alternative structures, leading to an identification
443 of the main folding funnels. Subsequent all atom simulations can then be used to
444 investigate details on the energy landscape, seeded by the structures obtained from the
445 coarse-grained simulations.

446 With this approach in mind, we recently started investigating the frameshifting
447 pseudoknot of SARS-CoV-2, for which a structure is known experimentally but for which
448 both experimental and simulation data suggest the existence of alternative structures. We
449 first simulated the system at a relatively high temperature with the CG model to generate
450 seeds for DPS in order to speed up the energy landscape exploration. Then, using discrete
451 pathsampling, a search for the conversion path between the native structure and a
452 proposed structure lacking the characteristic pseudoknot was initiated with these seeds.
453 Given the size of the system, simulations are computationally very demanding and still
454 ongoing, but preliminary results show the possible conversion path between the two
455 states (Fig.6).

456



457
458
459

Figure 6: Sample structures on the conversion pathway between the native state of the frameshifting pseudoknot of SARS-CoV-2 (left) and an alternative structure with no pseudoknot (right).

460 Another research direction is based on the extensive conformational sampling and access
461 to free-energy landscape explorations provided by H-REX, which could offer decisive
462 insights into key phenomena related to the RNA World hypothesis and the origins of life,
463 as currently studied by some of us. Previous studies on protein enzyme systems have
464 shown the crucial importance of proper conformational sampling of the reactant and
465 product states to understand the chemical reactivity of these biological objects (Maffucci,
466 Laage, Sterpone, et al. 2020). We thus aim at understanding how a ribozyme's accessible
467 conformations can affect its reactivity. Secondly, the end product of template-based RNA
468 replication in abiotic conditions is an RNA dimer. However, these are known to be very
469 stable constructs, with high denaturation temperatures. Inspired by the use of the REST2
470 strategy for the study of protein melting properties (Maffucci, Laage, Stirnemann, et al.
471 2020; Stirnemann and Sterpone 2015; Stirnemann and Sterpone 2017), we are currently
472 trying to understand how RNA duplexes separate upon temperature increase, and how
473 this depends on the strand sequence.

474 While many computational methods exist to study biomolecules, the challenges
475 encountered by the complexity of RNA folding means that the best strategy for
476 computational studies to yield useful biological insight, rests on the combination of
477 multiple approaches to overcome individual shortcomings and access time and size scales
478 otherwise inaccessible. While data-based structural predictions are important, they
479 require the additional insight from physical modelling, especially to understanding the
480 dynamic, polymorphic nature of RNA. Simulations of RNA have been used for decades, but
481 the maturity of many methods and the growing understanding of RNA means that a new
482 chapter of research has opened up, where computational approaches, if used properly,
483 will routinely provide exciting insights into the nature of RNA.

484 **Author Contributions**

485 KR, GS, PF and SP all contributed to the developments of the various methods presented
486 in the manuscript and all contributed to its writing. SP conceived the article and made the
487 figures.

488 Financial Support

489 KR is funded by the Cambridge Philosophical Society. KR and SP thank Université Paris
490 Cité for a visiting fellowship for KR. Some of the research mentioned here has received
491 funding from the European Research Council under the European Union's Eighth
492 Framework Program (H2020/20142020)/ERC Grant Agreement No. 757111 (G.S.). This
493 work was also supported by the "Initiative d'Excellence" program from the French State
494 (Grant "DYNAMO", ANR-11-LABX-0011-01 to GS). SP is thankful for the computing time
495 allocated to the French national computing grant A0090710584. This work was partially
496 supported by a STSM Grant from COST Action CA17139 (eutopia.unitn.eu) funded by
497 COST (www.cost.eu).

498 Conflicts of Interest

499 KR, GS and SP do not have any conflict of interest. P.F. is co-founder and shareholder of
500 Sibylla Biotech SPA, a company exploiting molecular simulations to perform early-stage
501 drug discovery.

502 Data availability statement

503 Simulation data is available through links relative to the original articles presenting the
504 material.

505 References

- 506 A Beccara, S., Fant, L., & Faccioli, P. (2015). Variational scheme to compute protein
507 reaction pathways using atomistic force fields with explicit solvent. Physical
508 Review Letters, *114*(9), 098103.
- 509 Baquero-Perez, B., Antanaviciute, A., Yonchev, I. D., Carr, I. M., Wilson, S. A., & Whitehouse,
510 A. (2019). The tudor snd1 protein is an m6a rna reader essential for replication
511 of kaposi's sarcoma-associated herpesvirus. eLife, *8*, e47261.
- 512 Bartolucci, G., Orioli, S., & Faccioli, P. (2018). Transition path theory from biased
513 simulations. Journal of Chemical Physics, *149*(7), 072336.
- 514 Biyun, S., Cho, S. S., & Thirumalai, D. (2011). Folding of human telomerase rna
515 pseudoknot using ion-jump and temperature-quench simulations. Journal of the
516 American Chemical Society, *133*(50), 20634–20643.
- 517 Bottaro, S., Nichols, P. J., Vögeli, B., Parrinello, M., & Lindorff-Larsen, K. (2020). Integrating
518 NMR and simulations reveals motions in the UUCG tetraloop. Nucleic Acids
519 Research, *48*(11), 5839–5848. <https://doi.org/10.1093/nar/gkaa399>
- 520 Bourbigot, S., Dock-Bregeon, A.-C., Eberling, P., Coutant, J., Kieffer, B., & Lebars, I. (2016).
521 Solution structure of the 5'-terminal hairpin of the 7SK small nuclear RNA. RNA,
522 *22*(12), 1844–1858.

- 523 Brillet, K., Martinez-Zapien, D., Bec, G., Ennifar, E., Dock-Bregeon, A.-C., & Lebars, I. (2020).
524 Different views of the dynamic landscape covered by the 5'-hairpin of the 7SK
525 small nuclear RNA. RNA, 26(9), 1184–1197.
- 526 Bryngelson, J. D., Onuchic, J. N., Socci, N. D., & Wolynes, P. G. (1995). Funnels, pathways,
527 and the energy landscape of protein folding: A synthesis. Proteins, 21(3), 167–
528 195.
- 529 Bryngelson, J. D., & Wolynes, P. G. (1987). Spin glasses and the statistical mechanics of
530 protein folding. Proceedings of the National Academy of Sciences USA, 84, 7524–
531 7528.
- 532 Burge, S., Parkinson, G. N., Hazel, P., Todd, A. K., & Neidle, S. (2006). Quadruplex dna:
533 Sequence, topology and structure. Nucleic Acids Research, 34(19), 5402–5415.
- 534 Cameron, M., & Vanden-Eijnden, E. (2014). Flows in complex networks: Theory,
535 algorithms, and application to Lennard-Jones cluster rearrangement. Journal of
536 Statistical Physics, 156(3), 427–454.
- 537 Camilloni, C., Broglia, R. A., & Tiana, G. (2011). Hierarchy of folding and unfolding events
538 of protein g, ci2, and acbp from explicit-solvent simulations. Journal of Chemical
539 Physics, 134(4), 045105.
- 540 Cho, S. S., Pincus, D. L., & Thirumalai, D. (2009). Assembly mechanisms of rna pseudoknots
541 are determined by the stabilities of constituent secondary structures.
542 Proceedings of the National Academy of Sciences 106(41), 17349–17354.
- 543 Cragolini, T., Chakraborty, D., Šponer, J., Derreumaux, P., Pasquali, S., & Wales, D. J.
544 (2017). Multifunctional energy landscape for a dna g-quadruplex: An evolved
545 molecular switch. Journal of Chemical Physics, 147(15), 152715.
- 546 Cragolini, T., Laurin, Y., Derreumaux, P., & Pasquali, S. (2015). Coarse-grained hire-rna
547 model for ab initio rna folding beyond simple molecules, including noncanonical
548 and multiple base pairings. Journal of Chemical Theory and Computation, 11(7),
549 3510–3522.
- 550 Denesyuk, N. A., & Thirumalai, D. (2011). Crowding promotes the switch from hairpin to
551 pseudoknot conformation in human telomerase rna. Journal of the American
552 Chemical Society, 133(31), 11858–11861.
- 553 E, W., & Vanden-Eijnden, E. (2010). Transition-path theory and path-finding algorithms
554 for the study of rare events. Annual Review of Physical Chemistry, 61, 391–420.
- 555 Egloff, S., C, S., & Kiss, T. (2018). 7sk small nuclear rna, a multifunctional transcriptional
556 regulatory
557 rna with gene-specific features. Transcription, 9, 95–101.
- 558 Fay, M. M., Lyons, S. M., & Ivanov, P. (2017). RNA G-quadruplexes in biology: Principles
559 and molecular mechanisms. Journal of Molecular Biology, 429(14), 2127–2147.
- 560 Ferreira, D. U., Komives, E. A., & Wolynes, P. G. (2014). Frustration in biomolecules.
561 Quarterly Review in Biophysics, 47, 285–363.
- 562 Fiorini, G., Klein, M. L., & Hénin, J. (2013). Using collective variables to drive molecular
563 dynamics simulations. Molecular Physics, 111, 3345–3362.

- 564 Garst, A. D., Edwards, A. L., & Batey, R. T. (2011). Riboswitches: Structures and
565 mechanisms. Cold Spring Harbor Perspectives in Biology, *3*(6).
- 566 Gavory, G., Symmons, M. F., Ghosh, Y. K., Klenerman, D., & Balsubramanian, S. (2006).
567 Structural analysis of the catalytic core of human telomerase rna by fret and
568 molecular modeling.
569 Biochemistry, *45*(44), 13304–13311.
- 570 Gillet, N., Bartocci, A., & Dumont, E. (2021). Assessing the sequence dependence of
571 pyrimidine–pyrimidone (6–4) photoproduct in a duplex double-stranded dna: A
572 pitfall for microsecond range simulation. The Journal of Chemical Physics, *154*,
573 135103.
- 574 Guito, J., & Lukac, D. M. (2012). KSHV RTA promoter specification and viral reactivation.
575 Frontiers in Microbiology, *3*, 30.
- 576 Halvorsen, M., Martin, J. S., Broadaway, S., & Laederach, A. (2010). Disease-associated
577 mutations that alter the rna structural ensemble. PLoS Genetics, *6*(8), e1001074.
- 578 Jaeger, L., Verzemnieks, E., & Geary, C. (2009). The UA_handle: A versatile submotif in
579 stable rna architectures. Nucleic Acids Research, *37*(1), 215–230.
- 580 Joseph, J. A., Röder, K., Chakraborty, D., Mantell, R. G., & Wales, D. J. (2017). Exploring
581 biomolecular energy landscapes. Chemical Communications, *53*, 6974–6988.
- 582 Kim, N.-K., Zhang, Q., Zhou, J., Theimer, C. A., Peterson, R. D., & Feigon, J. (2008). Solution
583 structure and dynamics of the wild-type pseudoknot of human telomerase rna.
584 Journal of Molecular Biology, *384*(5), 1249–1261.
- 585 Kolesnikova, S., & Curtis, E. A. (2019). Structure and function of multimeric g-
586 quadruplexes. Molecules, *24*(17), 3074.
- 587 Kührová P., Best, R. B., Bottaro, S., Bussi, G., Šponer, J., Otyepka, M., & Banáš, P. (2016).
588 Computer folding of rna tetraloops: Identification of key force field deficiencies.
589 Journal of Chemical Theory and Computation, *12*(9), 4534–4548.
- 590 Lazzeri, G., Micheletti, C., Pasquali, S., & Faccioli, P. (2022). Rna folding landscapes from
591 explicit
592 solvent all-atom simulations. [arXiv:2205.12603](https://arxiv.org/abs/2205.12603).
- 593 Lebars, I., Martinez-Zapien, D., Durand, A., Coutant, J., Kieffer, B., & Dock-Bregeon, A.-C.
594 (2010). HEXIM1 targets a repeated GAUC motif in the riboregulator of
595 transcription 7SK and promotes base pair rearrangements. Nucleic Acids
596 Research, *38*(21), 7749–7763.
- 597 Leontis, N. B., & Westhof, E. (2001). Geometric nomenclature and classification of rna base
598 pairs. RNA, *7*(4), 499–512.
- 599 Leopold, P. E., Montal, M., & Onuchic, J. N. (1992). Protein folding funnels: a kinetic
600 approach to the sequence-structure relationship. Proceedings of the National
601 Academy of Sciences USA, *89*(18), 8721–8725.
- 602 Li, J., & Chen, S.-J. (2021). RNA 3d structure prediction using coarse-grained models.
603 Frontiers in Molecular Biosciences, *8*, 720937.

- 604 Li, P. T., Viereg, J., & Tinoco, I. (2008). How rna unfolds and refolds. Annual Review of
605 Biochemistry, *77*, 77–100.
- 606 Lightfoot, H. L., Hagen, T., Tatum, N. J., & Hall, J. (2019). The diverse structural landscape
607 of quadruplexes. FEBS Letters, *593*(16), 2083–2102.
- 608 Liu, N., Zhou, K. I., Parisien, M., Dai, Q., Diatchenko, L., & Pan, T. (2017). N6-
609 methyladenosine alters RNA structure to regulate binding of a low-complexity
610 protein. Nucleic Acids Research, *45*(10), 6051–6063.
- 611 Lorenz, R., Wolfinger, M. T., Tanzer, A., & Hofacker, I. L. (2016). Predicting rna secondary
612 structures from sequence and probing data. Methods, *103*, 86–98.
- 613 Ma, Y., Monsavior, A., Pasquali, S., & Röder, K. (2021). Comparison of coarse-grained and
614 all-atom representations by explicit energy landscape explorations. chemRxiv,
615 PrePrint.
- 616 Maffucci, I., Laage, D., Sterpone, F., & Stirnemann, G. (2020). Thermal adaptation of
617 enzymes: Impacts of conformational shifts on catalytic activation energy and
618 optimum temperature. Chemistry-A European Journal, *26*(44), 10045–10056.
- 619 Maffucci, I., Laage, D., Stirnemann, G., & Sterpone, F. (2020). Differences in thermal
620 structural changes and melting between mesophilic and thermophilic
621 dihydrofolate reductase enzymes. Physical Chemistry Chemical Physics, *22*(33),
622 18361–18373.
- 623 Martinez-Zapien, D., Legrand, P., McEwen, A. G., Proux, F., Cragolini, T., Pasquali, S., &
624 DockBregon, A.-C. (2017). The crystal structure of the 5' functional domain of
625 the transcription riboregulator 7SK. Nucleic Acids Research, *45*(6), 3568–3579.
- 626 Mazzanti, L., Alferkh, L., Frezza, E., & Pasquali, S. (2021). Biasing rna coarse-grained
627 folding simulations with small-angle x-ray scattering data. Journal of Chemical
628 Theory and Computation, *17*(10), 6509–6521.
- 629 Mlýnský, V., & Bussi, G. (2018). Exploring rna structure and dynamics through enhanced
630 sampling simulations. Current Opinion in Structural Biology, *49*, 63–71.
- 631 Mlýnský, V., Janeček, M., Kührová, P., Fröhlking, T., Otyepka, M., Bussi, G., Banáš, P., &
632 Šponer, J. (2022). Toward convergence in folding simulations of rna tetraloops:
633 Comparison of enhanced sampling techniques and effects of force field
634 modifications. Journal of Chemical Theory and Computation, *18*(4), 2642–2656.
- 635 Nguyen, V. T., Kiss, T., Michels, A., & Bensaude, O. (2001). 7sk small nuclear rna binds to
636 and inhibits the activity of cdk9/cyclin t complexes. Nature, (414), 322–325.
- 637 Nonin-Lecomte, S., Felden, B., & Dardel, F. (2006). Nmr structure of the aquifex aeolicus
638 tmrna pseudoknot pk1: New insights into the recoding event of the ribosomal
639 trans-translation. Nucleic Acids Research, *34*(6), 1847–1853.
- 640 Olson, S. W., Turner, A.-M. W., Arney, J. W., Saleem, I., Weidmann, C. A., Margolis, D. M.,
641 Weeks, K. M., & Mustoe, A. M. (2022). Discovery of a large-scale, cell-state-
642 responsive allosteric switch in the 7sk rna using dance-map. Molecular Cell,
643 *82*(9), 1708–1723.

- 644 Onsager, L., & Machlup, S. (1951). Fluctuations and irreversible processes. The Physical
645 Review, 91, 1505.
- 646 Paci, E., & Karplus, M. (1999). Forced unfolding of fibronectin type 3 modules: An analysis
647 by biased molecular dynamics simulations. Journal of Molecular Biology, 288(3),
648 441–459.
- 649 Papoian, G. A. (2018). Coarse-grained modeling of biomolecules. CRC Press.
- 650 Pasquali, S., & Derreumaux, P. (2010). HiRE-RNA: A high resolution coarse-grained energy
651 model for RNA. Journal of Physical Chemistry B, 114(37), 11957–11966.
- 652 Pasquali, S., Frezza, E., & Barroso da Silva, F. (2019). Coarse-grained dynamic rna titration
653 simulations. Interface Focus, 9, 20180066.
- 654 Perez, A., Marchan, I., Svozil, D., Šponer, J., Cheatham, T., Laughton, C., & Orozco, M. (2007).
655 Refinement of the amber force field for nucleic acids: Improving the description
656 of alpha/gamma conformers. Biophysical Journal, 92, 3817–3829.
- 657 Rissone, P., Bizarro, C. V., & Ritort, F. (2022). Stem-loop formation drives rna folding in
658 mechanical unzipping experiments. Proceedings of the National Academy of
659 Science USA, 119(3), e2025575119.
- 660 Röder, K., Barker, A. M., Whitehouse, A., & Pasquali, S. (2022). Investigating the structural
661 changes due to adenosine methylation of the kaposi's sarcoma-associated herpes
662 virus orf50 transcript. PLoS Computational Biology, 18(5), e1010150.
- 663 Röder, K., & Wales, D. J. (2018). Evolved minimal frustration in multifunctional
664 biomolecules. Journal of Physical Chemistry B, 122(49), 10989–10995.
- 665 Röder, K., Joseph, J. A., Husic, B. E., & Wales, D. J. (2019). Energy landscapes for proteins:
666 From single funnels to multifunctional systems. Advanced Theory and
667 Simulations, 2, 1800175.
- 668 Röder, K., & Pasquali, S. (2021). Rna modelling with the computational energy landscape
669 framework. In L. Ponchon (Ed.), Rna scaffolds (pp. 49–66). Humana.
- 670 Röder, K., Stirnemann, G., Dock-Bregeon, A.-C., Wales, D. J., & Pasquali, S. (2020). Structural
671 transitions in the rna 7sk 5' hairpin and their effect on hexim binding. Nucleic
672 Acids Research, 48(1), 373–389.
- 673 Saldi, T., Riemondy, K., Erickson, B., & Bentley, D. L. (2021). Alternative RNA structures
674 formed during transcription depend on elongation rate and modify RNA
675 processing. Molecular Cell, 81(8), 1789–1801.
- 676 Sato, K., & Kato, Y. (2022). Prediction of rna secondary structure including pseudoknots
677 for long
678 sequences. Briefings in Bioinformatics, 23(1), 1–9.
- 679 Schlick, T., Zhu, Q., Jain, S., & Yan, S. (2021). Structure-altering mutations of the sars-cov-2
680 frameshifting rna element. Biophysical Journal, 120(6), 1040–1053.
- 681 Šponer, J., Bussi, G., Krepl, M., Banáš, P., Bottaro, S., Cunha, R. A., Gil-Ley, A., Pinamonti,
682 G., Poblete, S., Jurečka, P., Walter, N. G., & Otyepka, M. (2018). RNA structural
683 dynamics as captured by molecular simulations: A comprehensive overview.
684 Chemical Reviews, 118(8), 4177–4338.

- 685 Stadlbauer, P., Mazzanti, L., Cragolini, T., Wales, D. J., Derreumaux, P., Pasquali, S., &
686 Šponer, J.(2016). Coarse-grained simulations complemented by atomistic
687 molecular dynamics provide new insights into folding and unfolding of human
688 telomeric G-quadruplexes. Journal of Chemical Theory and Com 12(12), 6077–
689 6097.
- 690 Stirnemann, G., & Sterpone, F. (2015). Recovering protein thermal stability using all-atom
691 hamiltonian replica-exchange simulations in explicit solvent. Journal of Chemical
692 Theory and Computation, 11(12), 5573–5577.
- 693 Stirnemann, G., & Sterpone, F. (2017). Mechanics of protein adaptation to high
694 temperatures. Journal of Physical Chemistry Letters, 8(23), 5884–5890.
- 695 Stombaugh, J., Zirbel, C. L., Westhof, E., & Leontis, N. B. (2009). Frequency and isostericity
696 of rna base pairs. Nucleic Acids Research, 37(7), 2294–2312.
- 697 Sugita, Y., & Okamoto, Y. (1999). Replica-exchange molecular dynamics method for
698 protein folding. Chemical Physics Letters, 314(1), 141–151.
- 699 Theimer, C. A., Blois, C. A., & Feigon, J. (2005). Structure of the human telomerase rna
700 pseudoknot
701 reveals conserved tertiary interactions essential for function. Molecular Cell,
702 17(5), 671–682.
- 703 Tiana, G., & Camilloni, C. (2012). Ratcheted molecular-dynamics simulations identify
704 efficiently the transition state of protein folding. Journal of Chemical Physics,
705 137(23), 235101.
- 706 Tinoco, I., & Bustamante, C. (1999). How rna folds. Journal of Molecular Biology, 293(2),
707 271–281. Vicens, Q., & Kieft, J. S. (2022). Thoughts on how to think (and talk) about rna
708 structure.
709 Proceedings of the National Academy of Science USA, 119(17), e2112677119.
- 710 Wales, D. J. (2002). Discrete path sampling. Molecular Physics, 100(20), 3285–3305.
- 711 Wales, D. J. (2004). Some further applications of discrete path sampling to cluster
712 isomerization. Molecular Physics, 102(9-10), 891–908.
- 713 Wales, D. J., & Salamon, P. (2014). Observation time scale, free-energy landscapes, and
714 molecular symmetry. Proceedings of the National Academy of Sciences USA,
715 111(2), 617–622.
- 716 Wang, L., Friesner, R. A., & Berne, B. (2011). Replica exchange with solute scaling: A more
717 efficient version of replica exchange with solute tempering (rest2). Journal of
718 Physical Chemistry B, 115(30), 9431–9438.
- 719 Wang, L., Liu, Y., Zhong, X., Liu, H., Lu, C., Li, C., & Zhang, H. (2019). Dmfold: A novel method
720 to predict rna secondary structure with pseudoknots based on deep learning and
721 improved base pair maximization principle. Frontiers in Genetics, 10, 143.
- 722 Wassarman, D. A., & Steitz, J. A. (1991). Structural analyses of the 7SK ribonucleoprotein
723 (RNP), the most abundant human small RNP of unknown function. Molecular and
724 Cellular Biology, 11(7), 3432–3445.
- 725 Yan, S., Zhu, Q., Jain, S., & Schlick, T. (2022). Length-dependent motions of sars-cov-2
726 frameshifting rna pseudoknot and alternative conformations suggest avenues for

- 727 frameshifting suppression. Research square, Preprint.
728 <https://doi.org/10.21203/rs.3.rs-1160075/v1>
- 729 Yang, Z., Zhu, Q., Luo, K., & Zhou, Q. (2001). The 7sk small nuclear rna inhibits the
730 cdk9/cyclin t1 kinase to control transcription. Nature, (414), 317–322.
- 731 Yu, A. M., Gasper, P. M., Cheng, L., Lai, L. B., Kaur, S., Gopalan, V., Chen, A. A., & Lucks, J. B.
732 (2021). Computationally reconstructing cotranscriptional rna folding from
733 experimental data reveals rearrangement of non-native folding intermediates.
734 Molecular Cell, *81*(4), 870–883.
- 735 Zaccara, S., Ries, R. J., & Jaffrey, S. R. (2019). Reading, writing and erasing mRNA
736 methylation. Nature Reviews Molecular Cell Biology, *20*(10), 608–624.
- 737 Zgarbová, M., Otyepka, M., Šponer, J., Mládek, A., Banáš, P., Cheatham, T. E., & Jurečka, P.
738 (2011).[✓] Refinement of the Cornell et al. Nucleic acids force field based on
739 reference quantum chemical calculations of glycosidic torsion profiles. Journal of
740 Chemical Theory and Computation, *7*(9), 2886–2902.
- 741 Zhao, Q., Zhao, Z., Fan, X., Yuan, Z., Mao, Q., & Yao, Y. (2021). Review of machine learning
742 methods for rna secondary structure prediction. PLoS Computational Biology,
743 *17*(8), e1009291.
- 744